NeuroImage 200 (2019) 607–620

Contents lists available at ScienceDirect

NeuroImage

journal homepage: www.elsevier.com/locate/neuroimage

Increased segregation of functional networks in developing brains

Wei He [a,b,*], Paul F. Sowman [a,b], Jon Brock [b], Andrew C. Etchell [b], Cornelis J. Stam [c], Arjan Hillebrand [c]

[a] Department of Cognitive Science, Australian Hearing Hub Level 3, 16 University Avenue, Macquarie University, NSW, 2109, Australia
[b] Australian Research Council Centre of Excellence in Cognition and Its Disorders, Australian Hearing Hub Level 3, 16 University Avenue, Macquarie University, NSW, 2109, Australia
[c] Amsterdam UMC, Vrije Universiteit Amsterdam, Department of Clinical Neurophysiology and MEG Center, Amsterdam Neuroscience, De Boelelaan, 1117, Amsterdam, the Netherlands

A B S T R A C T

A growing literature conceptualises typical brain development from a network perspective. However, largely due to technical and methodological challenges inherent in paediatric functional neuroimaging, there remains an important gap in our knowledge regarding the typical development of functional brain networks in "pre-school" childhood (i.e., children younger than 6 years of age). In this study, we recorded brain oscillatory activity using age-appropriate magnetoencephalography in 24 children, including 14 preschool children aged from 4 to 6 years and 10 school children aged from 7 to 12 years. We compared the topology of the resting-state brain networks in these children, estimated using minimum spanning tree (MST) constructed from phase synchrony between beamformer-reconstructed time-series, with that of 24 adults. Our results show that during childhood the MST topology shifts from a star-like (centralised) toward a more line-like (de-centralised) configuration, indicating the functional brain networks become increasingly segregated. In addition, the increasing global network segregation is frequency-independent and accompanied by decreases in centrality (or connectedness) of cortical regions with age, especially in areas of the default mode network. We propose a heuristic MST model of "network space", which posits a clear developmental trajectory for the emergence of complex brain networks. Our results not only revealed topological reorganisation of functional networks across multiple temporal and spatial scales in childhood, but also fill a gap in the literature regarding neurophysiological mechanisms of functional brain maturation during the preschool years of childhood.

1. Introduction

The human brain undergoes profound changes in its rhythmic electrical activity (i.e., neuronal oscillations; Buzsaki, 2006; Buzsaki and Draguhn, 2004) during childhood development (Uhlhaas et al., 2010). Such developmental change is far from random and has been shown to a large degree to manifest within so-called "resting-state networks", where anatomically disparate brain regions exhibit highly synchronised activity even in the absence of external stimuli (Grayson and Fair, 2017). At the network level, this is a process that requires an ongoing functional balance between the integration of converging information from distributed brain regions (Fair et al., 2009; Marek et al., 2015) and, at the same time, the segregation of divergent specialised information streams (Baum et al., 2017; Cao et al., 2017; Fair et al., 2007).

The topology of networks can be characterised using graph theory (Newman, 2010; Sporns, 2011), for which, at the macroscopic level, brain regions are represented as nodes and functional connections between these regions as edges (or links). A functional connection between brain areas is typically defined as a statistical dependency between time series of neuronal activity (Friston, 1994). Over the last decade, magnetoencephalography (MEG) and electroencephalography (EEG) have been increasingly used to measure neuronal oscillations and to track the highly-dynamic functional connections that occur between cortical regions. Such endeavour in the study of neurodevelopment has been further facilitated by the resting-state assessment of brain function (i.e., in the absence of a task; see also Van Diessen et al., 2015). Resting-state assessments are especially important in paediatric neuroimaging because the participation of children in such studies is relatively easy to obtain compared to task-based studies. Studying resting-state brain functions have been enabled important insights into the intrinsic properties of the human brain that associate with task-relevant behavioural performance in both normal and abnormal conditions (e.g., Cole et al., 2012; van den Heuvel et al., 2008).

Modern network science has revealed that normal brain networks exhibit fundamental properties of three canonical network extremes - *a random network* (Erdös and Rényi, 1959), a locally connected *regular network* (Mulder, 1992), and a *scale-free network* with a small number of highly connected "hubs" (Barabasi and Albert, 1999). Adult brain

* Corresponding author. Department of Cognitive Science, Australian Hearing Hub Level 3, 16 University Avenue, Macquarie University, NSW, 2109, Australia.
E-mail address: wei.he@mq.edu.au (W. He).

https://doi.org/10.1016/j.neuroimage.2019.06.055
Received 11 October 2018; Received in revised form 31 March 2019; Accepted 24 June 2019
Available online 2 July 2019
1053-8119/

networks also display *hierarchical modularity* (Meunier et al., 2009; Stam, 2014; Wig, 2017), in which major functional systems such as the default mode network support specific cognitive functions (Bullmore et al., 2009; Fornito et al., 2011; Power et al., 2011). A heuristic model of complex brain networks has been proposed to characterise the properties of real brain networks in an abstract "network space" defined by the four network models (i.e., random, regular, scale-free, and hierarchical modular networks; Stam and van Straaten, 2012). This heuristic model of "network space" suggests that the *hierarchical modular network* is an "optimal brain state" for healthy brain networks, and the other three extreme networks represent network configurations that exist in pathological brain states (Stam, 2014; Stam and van Straaten, 2012).

Although it is generally assumed that an optimal network organisation emerges during typical brain development (Stam, 2014), there is little agreement about the exact nature of this process. For instance, the healthy adult brain displays so-called "small-worldness" (Watts and Strogatz, 1998), i.e. a network topology that falls between the regular and random models, exhibiting a delicate balance between dense local connectivity and a sufficient number of long-distance connections (Douw et al., 2011; van den Heuvel et al., 2008). Some studies indicate that brain networks are initially random-like and transition toward "small--worldness" over time (Boersma et al., 2011; van den Heuvel et al., 2015). Others argue that network development starts out in a more lattice-like, ordered and locally connected configuration (Fair et al., 2009; Yap et al., 2011). Such discrepancies in the findings of these aforementioned developmental network studies can probably be ascribed to a network comparison problem, i.e., inconsistancies in the statistical comparison of brain networks estimated from different graph theoretical methods, for example the use of weighted versus unweighted graphs, the use of different thresholds on graphs, and/or the normalisation of graphs via random surrogates (van Wijk et al., 2010). An approach to get around the network comparison problem is through the use of the minimum spanning tree (MST), which constructs a unique and acyclic sub-network with a fixed number of connections (Stam et al., 2014; Tewarie et al., 2015). Importantly, the unique subset of connections in the MST forms the critical backbone of the original network (Van Mieghem and Magdalena, 2005; Wang et al., 2008), over which all information in the original graph flows (Van Mieghem and van Langen, 2005). Moreover, the MST has also been shown to form the critical backbone of the human brain connectome (van Dellen et al., 2018).

Recent developmental studies have identified frequency specific trajectories of brain network maturation using the MST. An EEG study of 139 infants aged 1–6 days reported that MST measures in infants correlate with gestational age (Toth et al., 2017), indicating that functional brain networks shift from a star-like (centralised) configuration toward a more line-like (de-centralised) configuration in the theta band during the first week of life (when compared to random control networks). Such reorganisation of the topological structure in resting-state EEG networks has also been found in the alpha band in 227 children during a 2-year period between 5 and 7 years of age (Boersma et al., 2013), suggesting a continuous trajectory of the network topology moving from "star-like" to "line-like" in typical early brain development. However, the sensor level network approaches employed in these EEG studies should be interpreted with caution as they may have been affected by spatial under sampling and/or volume conduction/field spread (Antiqueira et al., 2010; Dominguez et al., 2007; Lai et al., 2017; Schoffelen and Gross, 2009).

Even though the developing brain has increasingly been studied from a network perspective, most studies to date have focused on children older than 6 years or younger than 3 years of age (Grayson and Fair, 2017). There exists only a single EEG study that has looked at network reorganisation in children aged between 2 and 6 years (Bathelt et al., 2013). Using conventional graph theoretical measures applied to broadband (1–40 Hz) data, increased nodal degree and maximum betweenness centrality, as well as decreased path length, were found, suggesting an increase in network integration occurs during the preschool years across frequencies.

MEG signals, as opposed to EEG, are relatively unperturbed by the biological tissues interposed between the electrical sources in the brain and the extra-cranial MEG sensors (Baillet, 2017). This simplifies the inverse problem, meaning that highly-resolved neuronal time series (millisecond resolution) can be extracted from source estimates with good spatial resolution (varying from sub-millimetre to a few centimetres, see Hillebrand and Barnes, 2005; Troebinger et al., 2014). MEG therefore offers an excellent combination of temporal and spatial resolution. However, the fixed sensor geometries of standard MEG systems present a significant impediment to routine MEG experimentation on young children. Most commonly available MEG systems feature sensor arrays optimised for adult-sized heads which, when used on child-sized heads, generally results in poor data quality due to low signal to noise ratio and high co-registration error due to excessive head movement. This practical challenge has greatly restricted the usage of MEG in studying functional connectivity and brain networks in young populations.

To better understand how frequency-mediated functional brain networks develop from childhood to adulthood, the present study used MEG to collect resting-state electrophysiological signals from children whose ages spanned 4–12 years, as well as from adults. We utilised a paediatric MEG system for data collection in preschool children to address this particular challenge (He et al., 2014; Johnson et al., 2010). Based on limited M/EEG research in network maturation during childhood, we hypothesised that the healthy brain develops from a more random and integrated structure towards a configuration that offers a balance between *integration* and *segregation*. Specifically, we predict that: (1) functional networks become more segregated, shifting from a centralized to a de-centralized configuration; (2) individual brain regions become more diverse in their connectedness, i.e., centrality of brain regions increases for hubs (e.g., areas of the default mode network), but decreases in non-hub regions (e.g., primary visual regions); (3) global and regional network changes are the most profound in preschool years, i.e., differences between preschool children versus school children or adults will be more pronounced than those for school children versus adults; (4) network differences between age groups share the same profile across frequency bands, at least when comparing young children with other age groups (as reported in Bathelt et al., 2013).

2. Methods

2.1. Participants

Participants were controls who took part in a larger project on stuttering. The dataset consisted of MEG recordings collected from 28 children and 24 adults during the 3–5 min of eyes-open resting-state. Due to excessive head movement, incidental system noise or signs of drowsiness, data from 4 children were excluded. The present analyses were therefore completed on a total of 48 participants: 24 children aged from 4 to 12 years and 24 adults (40.6 ± 17.4 years, 16 males; age-range: 20–61 years). Children were further divided into two groups: a preschool children group from 4 to 6 years of age ($N = 10$, 5.4 ± 1.1 years, 5 males) and a school children group between 7 and 12 years of age ($N = 14$, 9.8 ± 1.5 years, 12 males).

The experimental procedures were approved by the Human Participants Ethics Committee at Macquarie University. Written informed consent was obtained from adults. Oral informed consent was obtained from children along with written informed consent obtained from their parents/guardians. Exclusion criteria were a history of neurological, psychiatric, or major medical disorders, including head injury, alcohol or drug abuse, and current treatment with vasoactive or psychotropic medication. All participants were remunerated for their participation.

2.2. Experimental procedures

Upon arriving at the laboratory, participants were familiarised with

the magnetically shielded room where they would be tested in a supine position. Prior to MEG measurements, five head position indicators (HPI) were attached to a tightly fitting elastic cap. The 3D locations of the HPIs, anatomical landmarks (nasion, and left and right pre-auricular points) and the shape of each participant's head were measured with a pen digitizer (Polhemus Fastrak, Colchester, VT).

Children in the preschool group were tested using a paediatric 125-channel whole-head gradiometer MEG system (Model PQ1064R-N2m, Kanazawa Institute of Technology/KIT, Kanazawa, Japan). All other participants were tested using the 160-channel whole-head gradiometer MEG system (Model PQ1160RN2, KIT, Kanazawa, Japan). The gradiometers of both systems have 50 mm baseline and 15.5 mm diameter coils, and are positioned in a glass fibre reinforced plastic cryostat for measurement of the normal component of the magnetic field from the human brain (Kado et al., 1999). In both systems, neighbouring channels are 38 mm apart and 20 mm from the outer dewar surface. The 125-channel dewar was designed to fit a maximum head circumference of 53.4 cm, accommodating more than 90% of heads of 5-year olds (see details in Johnson et al., 2010). Both systems were situated within the same magnetically shielded room and therefore environmental noise was comparable (see Supplementary Materials).

During MEG data acquisition, participants were asked to remain relaxed and awake with their eyes fixed on a white cross at the centre of a black 36 cm (width) x 24 cm (length) rectangular image with 4 × 4 degrees of visual angle. Visual display was presented on a screen mounted approximately 140 cm above the participant using video projectors situated outside the magnetically shielded room (child MEG projector: Sharp Notevision Model PG10S, Osaka, Japan; Adult MEG projector: InFocus Model IN5108, Portland, USA). An experienced researcher accompanied child participants in the magnetically shielded room to ensure their comfort and relaxation, and to reinforce the need to minimise movement during the MEG recording. Eye opening was continuously monitored as a means of assessing the drowsiness of the participant so that any affected data could be removed from further analysis. This was done for the child participants by the experimenter who accompanied them in the magnetically shielded room, and for the adult participants by an experimenter monitoring a CCTV feed from the magnetically shielded room. An overview of the child-friendly experimental protocol can be found in the video article (Rapaport et al., 2019).

2.3. MEG data pre-processing

MEG data were acquired at a sampling frequency of 1000 Hz and with an online bandpass filter of 0.03–200 Hz. Head positions were measured at the beginning and end of the acquisition session.

The Yokogawa/KIT MEG data were firstly converted to a CTF data format using the *BrainWave* toolbox developed at the Hospital for Sick Children in Canada (http://cheynelab.utoronto.ca, version 3.3beta, see Cheyne et al., 2014 for details). Then, the CTF compatible MEG data were imported into and processed using DataEditor in the CTF MEG5 software (VSM MedTech Systems Inc., Coquitlam BC, Canada; Version 5.0.2). The continuous raw MEG data were firstly filtered from 0.5 to 100 Hz using bi-directional IIR Butterworth filters with DC removal and segmented into epochs of 4096 samples (= 4.096 s). A movement tolerance of 5 mm and 10 mm was used in adults and children, respectively, and epochs that were contaminated by head-movements or other physiological (e.g., muscle noise) or environmental artefacts were rejected by visual inspection. The cleaned datasets consisted on average of 23.8 (±3.02 S.D.) epochs for the children and 40 epochs (±0.02 S.D.) for the adults.

2.4. Head modelling and surrogate MRIs

For head model construction, obtaining individual structural magnetic resonance imaging (MRI) scans of children, especially of those aged below 6 years was deemed impractical. A "surrogate" MRI approach was therefore used to warp the adult Montreal Neurological Institute (MNI) template T1 structural brain image to each participant's digitised head shape via an iterative closest point algorithm implemented in *BrainWave* (see Cheyne et al., 2014 for details). MEG data from all adults and children were co-registered with the warped "surrogate" MRI using the digitised anatomical landmarks. The outline of the scalp from this co-registered "surrogate" MRI was extracted using the MRIViewer in the CTF MEG5 software (VSM MedTech Systems Inc., Coquitlam BC, Canada; Version 5.0.2) and then used to fit a multisphere volume conductor model (Huang et al., 1999). This model was subsequently used in the beamformer analysis described below.

2.5. Beamforming

An atlas-based beamforming approach (Hillebrand et al., 2012) was adopted to project sensor level MEG data into source (brain) space. The co-registered surrogate MRIs were normalised to the standard MNI (T1) template, using the SEG toolbox (Weiskopf et al., 2011) in SPM8. The automated anatomical labelling (AAL) atlas (Tzourio-Mazoyer et al., 2002) was used to label the voxels in a participant's normalised co-registered surrogate MRI, following which the centroid for each AAL regions of interest (80 ROIs; 78 cortical and bilateral hippocampal) was inversely transformed to native space (Hillebrand et al., 2016).

For each centroid, beamformer weights were computed using Synthetic Aperture Magnetometry (SAM; Robinson, 1999). This beamformer selectively weights the contribution from each MEG sensor to a voxel's activity based on the broad-band (0.5–48 Hz) data covariance matrix, which was computed from all selected time-series, the forward solution (lead field) for a dipolar source with optimum orientation at that location, and a unity noise covariance that was scaled by the smallest singular value in a decomposition of the data covariance matrix. The broad-band MEG data were subsequently projected through the normalised beamformer weights (Cheyne et al., 2007).

From the resulting time-series, the first 15 artefact-free epochs, containing 4096 samples (see Hillebrand et al., 2012 for MEG evidence that 15 epochs are sufficient for this atlas-based beamforming approach) were selected for further analyses of functional connectivity and network topology. These selected epochs were then band-pass filtered, using an offline discrete Fast Fourier Transform filter without phase distortion as implemented in the BrainWave toolbox (developed at VU University Medical Centre, Stam, [2014]; http://home.kpn.nl/stam7883/brainwave.html, version 0.9.152.4.1), into five canonical MEG frequency bands (delta: 0.5–4 Hz, theta: 4–8 Hz, alpha: 8–13 Hz, beta: 13–30 Hz, and low gamma: 30–48 Hz). Subsequently, the instantaneous phase for each time-series was determined by taking the augment of the analytic signal as computed using the Hilbert transform (Marple, 1999).

2.6. Connectivity analysis

Pair-wise frequency band-specific functional connectivity between the 80 ROIs was estimated using the phase lag index (PLI) for each of the 15 artefact-free epochs. PLI reflects the consistency in which one signal is phase leading or lagging with respect to another signal (Stam et al., 2007) and can be expressed as:

$$PLI = | < sign[\sin(\Delta\phi(t_k))] > |$$

where $\Delta\phi$ refers to the instantaneous phase difference between two time-series, t_k are discrete time steps calculated over all $k = 1 \ldots N$ samples, *sign* refers to the signum function, $<>$ and $||$ denote the mean and absolute value, respectively. Specifically, PLI quantifies phase synchronization as a measure of the asymmetry in the distribution of instantaneous phase differences between two time-series (in our case the beamformer reconstructed time-series for two ROIs). The value of PLI ranges from zero (random phase differences [no functional connectivity] or only zero-lag [mod π] connections) and one (perfect non-zero-lag synchrony). Because the effects of volume conduction result in zero-lag (mod π) phase

differences, PLI is insensitive to these effects at the cost of being blind to true zero-lag interactions. For each frequency band and each epoch, the 80 x 80 connectivity matrix of pairwise PLI values was computed. ROI-PLI was computed as the average PLI between a node and all other nodes, and whole-brain PLI was calculated as the average across all nodal PLI values.

2.7. Minimum spanning tree analysis

For each epoch and each participant separately, the minimum spanning tree (MST) sub-graph was constructed using the PLI connectivity matrix. The MST is constructed by connecting all n nodes in such a way that the cost (the sum of all link weights) is minimised without forming cycles. For computation of the MST, 1/PLI is used as the link weights since we are interested in the strongest connections in the network. MSTs were constructed in *BrainWave* by applying Kruskal's algorithm (Kruskal, 1956), which starts with an unconnected network, adds the link with lowest weight, and then adds the link with next lowest weight if this does not create a loop, until all nodes are connected, thereby forming a tree consisting of $m = n - 1$ links.

Two extreme tree topologies exist: (1) a line-like tree (A in Fig. 1) where all nodes are connected to two other nodes with the exception of the two, so-called, leaf-nodes at either end that have only one link, and (2) a star-like tree (C in Fig. 1) where all leaves are connected to one central node. There are many different tree types between these two extremes (e.g., B in Fig. 1). The tree topology can be characterised with various measures (Boersma et al., 2013):

Global MST network measures are informative about the functional integration and segregation of the entire network. Five different global MST measures were used here: (1) the "Leaf Fraction" is computed as the number of leaf nodes, divided by the total number of nodes; (2) the "Diameter" is the longest shortest path between any two nodes, where the shortest path is defined as the path with smallest number of links between two nodes; (3) the "Tree Hierarchy" was introduced (Boersma et al., 2013) to describe a balance between a small Diameter without overloading central nodes in the tree (Fig. 1). It is defined as $T_H = \frac{l}{2mBC_{max}}$, where l is the leaf number and BC_{max} represents the maximal betweenness centrality in the tree. In a line-like tree, $l = 2$ and with m approaching infinity, T_H approaches 0; and in a star-like tree, $l \approx m$, so T_H approaches 0.5; for l between these two extremes, T_H can have higher values (with an upper bound of 1); (4) the "Degree Correlation" or R is an index of whether the degree of a node is correlated with the degree of its neighbouring nodes (Van Mieghem et al., 2010); (5) "Kappa" (also called degree divergence; Barrat et al., 2008) measures the broadness of the degree distribution, and it is high in graphs with a scale-free degree distribution, and low in graphs with a degree distribution that approaches the normal distribution. Kappa also relates to network robustness – high kappa reflects high resilience against random damage in networks.

Nodal MST network measures capture the importance of a node within the network. Three different nodal measures for centrality ("hubness") were used: (1) the "Degree" is the number of connections of a node to its neighbouring nodes; (2) the "Betweenness Centrality" is the fraction of shortest paths that pass through a node; (3) the "Eccentricity" of a node is the longest shortest path between a node and any other node, and is low if the node is central in the graph (Bullmore and Sporns, 2012).

2.8. Statistical analysis

Statistical analyses were performed using permutation testing as implemented in the Resampling Statistical Toolkit for Matlab 2016a. We used 50,000 permutations of group membership to empirically approximate the distribution for the null hypothesis (i.e., no difference between groups) for each contrast. For each permutation, the F/t values were derived for a contrast of interest, and any F/t values for the original data that exceeded the significance threshold for the F/t distribution were deemed reliable. Furthermore, p values were corrected for multiple comparisons at the threshold of 0.05 using the false discovery rate (FDR; Benjamini and Hochberg, 1995). Effect sizes for all comparisons were estimated by Hedges's g (small effects: ±0.2, medium: ±0.5, large: ±0.8; Hedges, 1981) using the measures-of-effect-size-toolbox in Matlab (achieved statistical power for all significant results can be found in Table S8 in the Supplementary Materials).

For each frequency band and each participant separately, whole-brain PLI was averaged over the 15 epochs per participant. The ROI-PLI values, global and nodal MST measures were averaged over 15 epochs, yielding

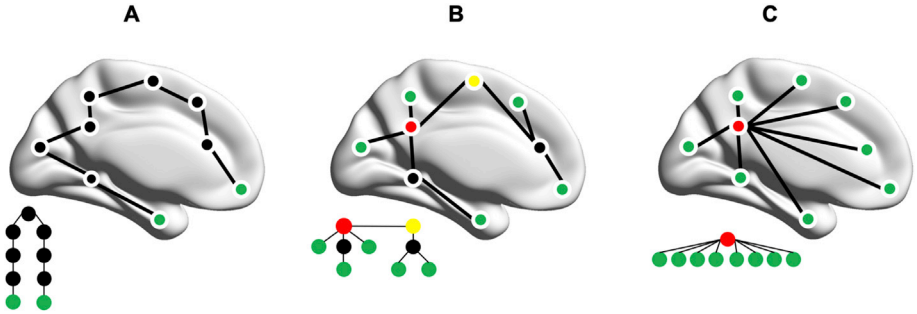

Fig. 1. Minimum spanning tree (MST) topology and hierarchy of three representative tree models. Top panel: (A) a line-like tree, and (C) a star-like tree; (B) an intermediate configuration between the two extremes. Nodes are indicated by circles; links by connecting lines. Green nodes are leaves, which have a Degree (i.e., number of links to neighbouring nodes) of 1; red nodes are hubs that have the highest Degree and Betweenness Centrality (i.e., the fraction of the smallest number of links between any two nodes in a network that pass through a node); the yellow node and the red node in B, have the lowest Eccentricity (i.e., the largest number of links required for a node reaching any other node in a network). The Diameter in B is 5 (i.e., the longest distance between any two nodes in a network). The three lower graphs are the same trees as those overlaid on the template brains above but represented in a way that illustrates that trees with more leaves have fewer layers (nodes with the lowest Eccentricity are placed on top). Network A requires many steps for an individual node, especially a leaf node in green, to connect to other nodes (low integration and high segregation). The steps required for nodes to connect with each other are fewer in C but the central hub (red node) is considered 'overloaded' (high integration but low segregation). The network between these extremes - network B - represents a hierarchical tree, which offers a balance between information integration and segregation.

80 ROI-PLI, five global MST, and 3 x 80 (= nodal MST measures x ROIs) values per participant for each frequency band, respectively.

Permutation tests were performed, for each frequency band separately, between adults and children (as a whole group), for the whole-brain PLI and the global MST measures (FDR corrected for the five global measures); if the whole-brain PLI or the global MST measures were significantly different in a specific frequency band, then the ROI-PLI and the nodal MST measures were compared (FDR corrected for three nodal measures x 80 ROIs). Second level permutation tests were performed in pairwise groups (school children versus preschool children, adults versus preschool children, and adults versus school children) for the whole-brain PLI and the global MST measures if adults and children (as a whole group) showed significant differences for these measures in any specific frequency band, and for the ROI-PLI and the nodal MST measures if these measures were significantly different in any specific frequency band between adults and children (as a whole group).

3. Results

3.1. Increased segregation of the large-scale functional networks

We first sought to understand whether functional networks become more segregated during childhood development. To this end, we calculated five global MST measures for each participant: Diameter, Leaf Fraction, Tree Hierarchy, Degree Correlation, and Kappa. Small Diameter and high Leaf Fraction are characteristic of a highly integrated network such as a star-like network (A in Fig. 1), whereas large Diameter and low Leaf Fraction are representative of a more line-like (de-centralised) network (C in Fig. 1). An optimal MST topology, requiring a small Diameter without overloading central nodes, is quantified by Tree Hierarchy (Boersma et al., 2013; Tewarie et al., 2015). Such a network topology also tends to have larger Degree Correlation and Kappa, suggesting it is resilient to random damage (Barrat et al., 2008; Van Mieghem et al., 2010).

Pairwise permutation comparison of the whole-brain PLI yielded no significant differences between groups for any of the five frequency bands ($p > 0.05$, FDR-corrected; $|g| = 0.001–0.43$), therefore no ROI-PLI comparisons were carried out. However, we found the five global MST measures were significantly different across all five frequency bands when comparing children (as a whole group) to adults: Kappa, Leaf Fraction, and Tree Hierarchy were higher, whereas Degree Correlation and Diameter were lower, in children (Fig. 2; $p < 0.001$, FDR-corrected; $|g| = 0.6–1.42$). These frequency-independent effects were all significant when contrasting preschool children with the other two age groups ($p < 0.001$, FDR-corrected; $|g| = 0.8–3.07$), but less so when comparing school children with adults. The school children were adult like for most global MST topological measures, apart from larger Leaf Fraction in the delta ($t = -2.19$, $p = 0.036$, FDR-corrected; $g = 0.7$) and beta ($t = -2.13$, $p = 0.041$, FDR-corrected; $g = 0.7$) bands, larger Kappa ($t = -2.56$, $p = 0.017$, FDR-corrected; $g = 0.84$) and Leaf Fraction ($t = -2.19$, $p = 0.036$, FDR-corrected; $g = 0.7$) in the theta band, and smaller Diameter ($t = 2.13$, $p = 0.023$, FDR-corrected; $g = -0.76$) but larger Leaf Fraction ($t = -2.13$, $p = 0.038$, FDR-corrected; $g = 0.7$) and Tree Hierarchy ($t = -3.06$, $p = 0.007$, FDR-corrected; $g = 1$) in the alpha band. Overall, the MST topology becomes more line-like and segregated across all frequency bands with increasing age (Fig. 3).

3.2. Regional de-centralisation correlates with increasing network segregation

Having established that the network topology is more segregated in adults than in children, we next investigated the centrality of brain

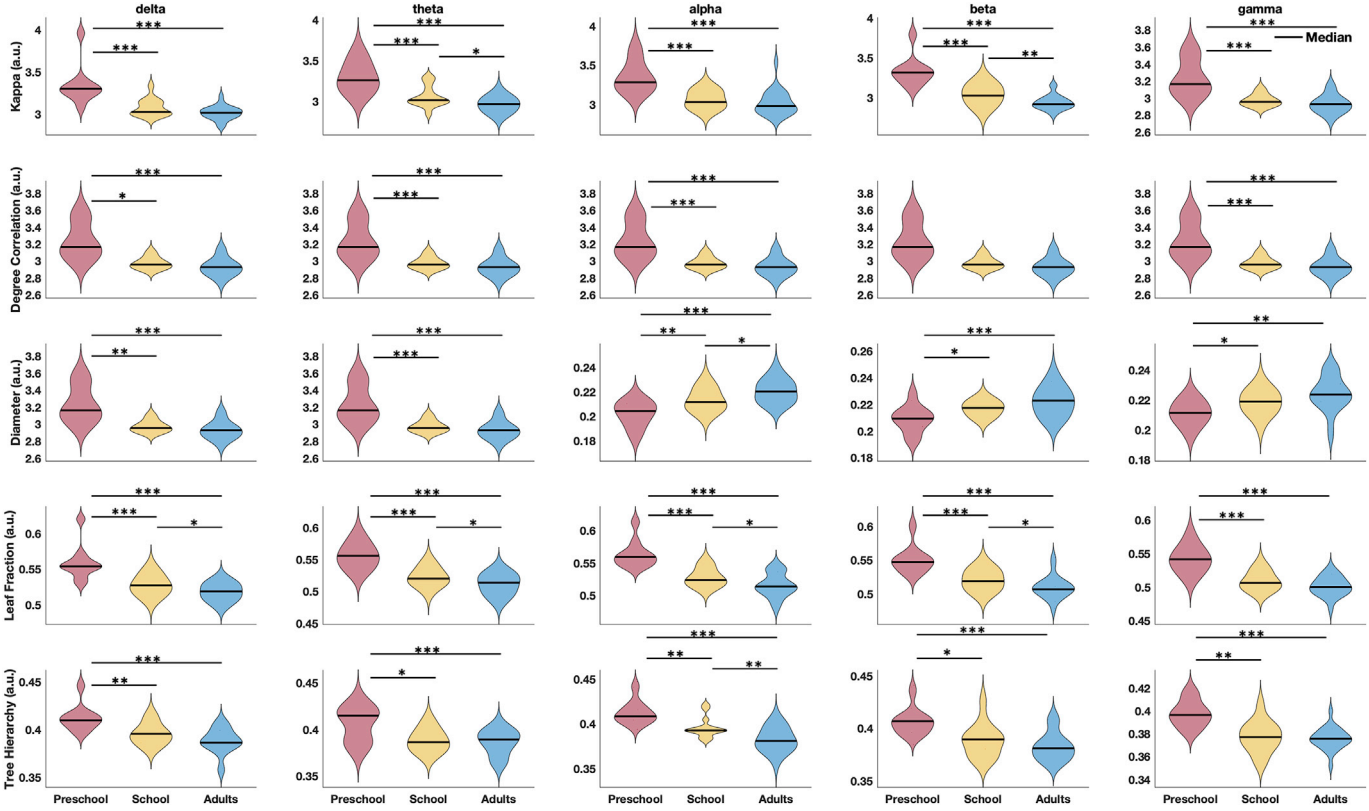

Fig. 2. Minimum spanning tree (MST) global metrics estimated from individual phase lag index adjacency matrices in the delta (0.5–4 Hz), theta (4–8 Hz), alpha (8–13 Hz), beta (13–30 Hz), and low gamma (30–48 Hz) bands for three age groups (preschool children in red, school children in yellow, and adults in blue). Error bars depict 95% confidence intervals estimated using bootstrapping with 1000 random iterations. * indicates statistically significant group differences ($p < 0.05$, 50,000 random permutations), ** for $p < 0.01$, and *** for $p < 0.001$.

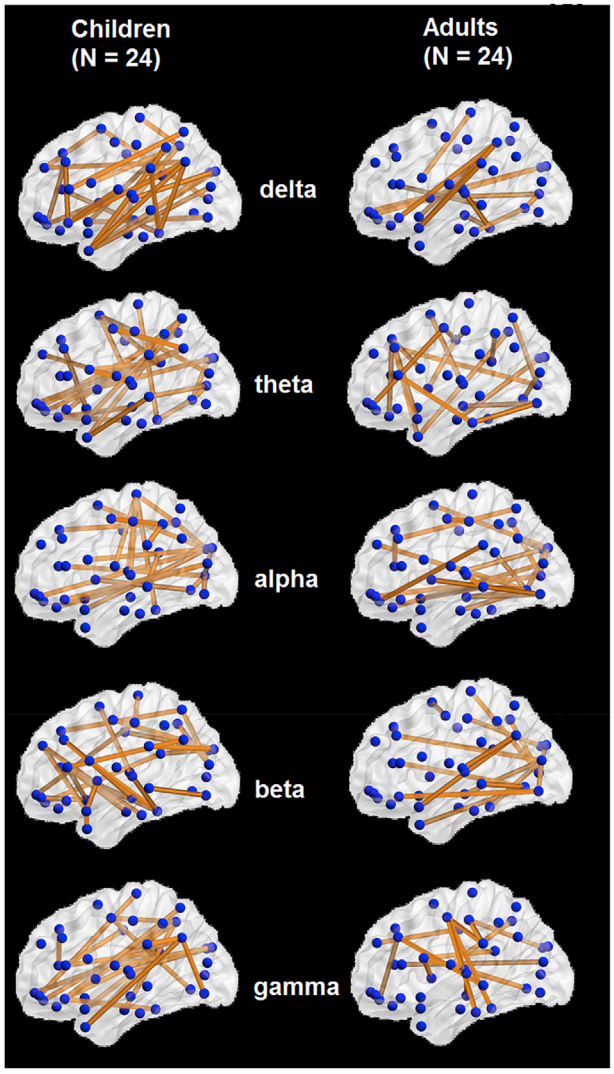

Fig. 3. Minimum spanning trees (MSTs) for adults (N = 24) and children (N = 24) in five frequency bands (delta: 0.5–4 Hz, theta: 4–8 Hz, alpha: 8–13 Hz, beta: 13–30 Hz, and low gamma: 30–48 Hz), displayed on a template brain with blue dots depicting nodes and yellow lines depicting functional connections. The MSTs depicted are estimated from averaged phase lag index adjacency matrices from adults (right panel) and children (left panel) for illustrative purposes only. All connections have the same weight. Transparency of the links implies the distance to the left cortical surface. All nodes are connected in MSTs. The nodes shown as disconnected are the ones that have no connection with the nodes in the left hemisphere.

regions. We calculated three nodal MST measures for each of the 80 regions in every participant: Degree, Betweenness Centrality, and Eccentricity. Larger Degree and Betweenness Centrality, but smaller Eccentricity characterise regions (or so-called "hubs") that play a central role in the network. We found that, even though there were no significant group differences for the Degree or Betweenness Centrality, the Eccentricity significantly increased from children (as a whole group) to adults, and from preschool children to adults in particular. The group differences for the Eccentricity (illustrated in Fig. 4 show pervasive changes in Eccentricity over the cortex (the full results are shown in Table 1).

When contrasting preschool children with adults, all 80 ROIs showed larger Eccentricity in the theta band mediated MSTs. In alpha, beta, and delta bands, most of the nodes showing larger Eccentricity were in fronto-parietal areas, followed by the nodes normally assigned to the default mode and parieto-temporal areas, and in hippocampal and occipital areas. About half of the nodes in the default mode, parieto-temporal, and the occipital areas showed larger Eccentricity in gamma mediated MSTs in preschool children than in adults.

When comparing school children to adults, most of the nodes showing larger Eccentricity were in the default mode, parieto-temporal, occipital, and fronto-parietal areas in the alpha band mediated MSTs. Nodes from the default mode, parieto-temporal and occipital areas showed larger Eccentricity in the theta band, and those from the fronto-parietal, parieto-temporal, and hippocampal areas, as well as the nodes from the default mode areas showed larger Eccentricity in the beta band in school children than in adults. Only nodes from occipital areas and the default mode areas showed larger Eccentricity in the gamma mediated MSTs, and no Eccentricity differences were found in the delta band when comparing school children with adults.

When contrasting adults to children (as a whole group), the group difference in Eccentricity was found mostly in nodes from the fronto-parietal areas, followed by those from default mode, parieto-temporal, occipital and hippocampal areas in delta-to-gamma mediated MSTs.

To provide a closer inspection of the overall pattern for the group differences across the five frequency bands, we collapsed the Eccentricity differences in such a way that a value of zero was assigned to any regions if the difference in the eccentricity was not significant in any of the five bands. The last row in Fig. 4 shows that the left fronto-parietal areas and the left dorsal part of the default mode areas consistently differed between adults and children (as a whole group). Additionally, the (pre-) motor and temporal areas also differed between the preschool children and adults across all five frequency bands.

4. Discussion

In this cross-sectional MEG study, we examined the development of frequency-specific functional brain networks by comparing children ranging from 4 to 12 years of age to adults. Globally, MST networks have smaller Diameter and Degree Correlation but larger Leaf Fraction, Kappa, and Tree Hierarchy in children than in adults across all frequency bands, suggesting that the topology of functional brain networks becomes segregated via a transition from a star-like (centralised) configuration toward a more line-like (de-centralised) configuration during childhood development. At the regional level, we found smaller Eccentricity across all five frequency bands for a distributed set of brain regions when comparing children to adults, indicating that most brain regions become functionally specialised and less central. This pervasive decrease in centrality (or connectedness) of cortical regions indicates that the reorganisation of network topology is not routed via a few hub regions. Moreover, our PLI findings failed to show any group differences, thereby indicating the network topology changes in the absence of changes in functional connectivity itself (for a similar dissociation between PLI and MST results see Fraga Gonzalez et al., [2016]).

Our global MST results are in line with our hypothesis of the "random-to-ordered" maturational trajectory of network topology during typical brain development. The observed smaller Diameter and larger Leaf Fraction in children compared to adults is in broad agreement with two earlier EEG studies that used a similar approach at the sensor level, where smaller Diameter and larger Leaf Fraction (compared with random control networks) were also found in newborn infants (Toth et al., 2017), as well as in children aged 5 years compared with 7-year-olds (Boersma et al., 2013). In previous simulations (Tewarie et al., 2015), increasing Diameter and decreasing Leaf Fraction have also been found to associate with "random-to-order" network topology changes. Importantly, this is consistent with an earlier longitudinal EEG study (Boersma et al., 2011), which also found a similar transition from a more random topology toward a more regular topology with age (5–7 years compared to 16–18 years). We suspect that the increase in network diameter with age promotes long-range connections for communication between distant neuronal populations, whereas the decrease in leaf fraction with age indicates the appearance of locally specialised regions in segregated networks.

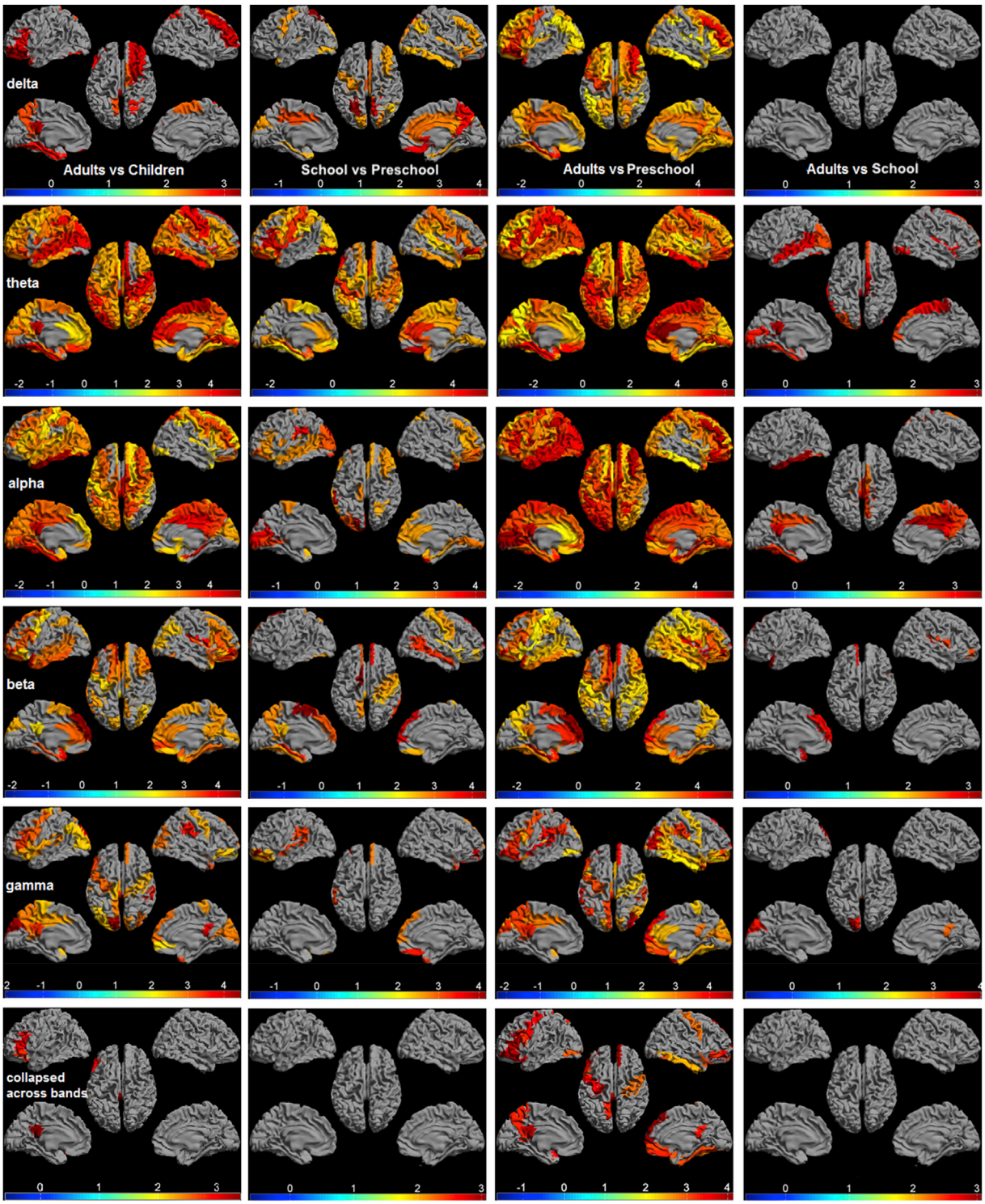

Fig. 4. Significant differences in the minimum spanning tree (MST) Eccentricity displayed as a color-coded map on the parcellated template brain, viewed from, in clockwise order, the left, top, right, right midline, and left midline. From left to right, pairwise differences (t-value, $p < 0.05$, FDR-corrected for three nodal MST measures x 80 ROIs) between adults and children, school children and preschool children, adults and preschool children, as well as adults and school children, are shown for all five frequency bands (delta: 0.5–4 Hz, theta: 4–8 Hz, alpha: 8–13 Hz, beta: 13–30 Hz, and low gamma: 30–48 Hz).

Globally, we also found a higher Kappa and lower Degree Correlation in children than in adults. Since Kappa is a measure of the degree diversity in a network, the decrease in Kappa with age is indicative of the network topology becoming less scale-free during development. In the simulation study of Tewarie et al. (2015), when rewiring a scale-free network to a random network, Kappa was found to decrease. Decrease in scale-freeness in functional brain networks with age seems to be at odds with findings from most adult studies, which indicate that the matured brain network is approximately "scale-free" (Sporns, 2013). However, Kappa is not strictly tied to "scale-freeness", but rather is a measure of the homogeneity of the degree distribution in the MST (especially in the case of small networks; Wang et al., 2009). Moreover, scale-freeness is a relative measure and depends on the reference model that the experimental model is compared with (Stam and van Straaten,

Table 1
Eccentricity differences between groups across all 80 regions of interest (ROIs) in the in five frequency bands (delta/δ: 0.5–4 Hz, theta/θ: 4–8 Hz, alpha/α: 8–13 Hz, beta/β: 13–30 Hz, and low gamma/γ: 30–48 Hz). Numbers in the table represent t values of significant group differences and bars indicate insignificant differences in Eccentricity from pairwise permutation comparisons ($p < 0.05$, FDR-corrected; 50000 random permutations).

	Pairwise Permutation Comparisons (FDR-corrected)																			
ROIs	Adults vs. Children					School vs. Preschool					Adults vs. Preschool					Adults vs. School				
Frequency Bands	δ	θ	α	β	γ	δ	θ	α	β	γ	δ	θ	α	β	γ	δ	θ	α	β	γ
Left Hemisphere																				
Gryus Rectus	-	3.9	-	-	-	-	3.0	-	-	-	2.8	5.2	2.9	-	-	-	-	-	-	-
Olfactory Cortex	-	2.8	-	2.9	-	-	-	-	-	-	2.9	3.2	2.9	3.3	-	-	-	-	-	-
Superior frontal gyrus, orbital part	2.8	3.1	-	3.3	-	-	3.9	-	-	2.5	3.0	4.3	-	3.2	-	-	-	-	-	-
Frontal gyrus, medial orbital part	-	3.2	3.1	-	-	-	2.5	-	-	-	-	4.5	3.9	-	-	-	-	-	-	-
Middle frontal gyrus, orbital part	3.3	3.3	-	3.7	-	-	3.8	3.2	-	4.2	4.3	4.8	3.4	4.3	3.9	-	-	-	-	-
Inferior frontal gyrus, orbital part	3.2	3.8	2.8	2.5	2.7	-	3.1	2.7	-	2.5	5.2	4.6	3.9	3.0	3.7	-	-	-	-	-
Superior frontal gyrus	-	2.8	-	3.2	-	-	3.2	-	-	-	2.5	4.1	2.8	3.5	-	-	-	-	-	-
Middle frontal gyrus	-	2.8	3.4	-	-	-	-	-	-	-	3.0	2.9	3.6	-	-	-	-	-	-	-
Inferior frontal gyrus, opercular part	-	-	2.6	3.4	3.2	-	3.2	-	-	-	3.3	3.2	2.9	3.9	2.7	-	-	-	-	-
Inferior frontal gyrus, triangular part	2.9	3.3	2.6	3.2	3.4	-	4.6	2.8	-	-	4.1	5.3	4.5	3.5	3.7	-	-	-	-	-
Superior frontal gyrus, medial	-	2.7	2.6	4.7	-	-	-	-	3.1	-	3.0	3.1	3.7	5.2	-	-	-	-	2.8	-
Supplementary motor area	-	3.3	3.4	2.8	-	-	2.5	-	4.4	-	3.3	3.8	4.1	4.0	-	-	-	-	-	-
Paracentral lobule	-	3.3	3.5	-	2.5	-	3.3	2.8	-	-	-	4.6	4.3	-	-	-	-	-	-	-
Precentral gyrus	-	2.7	3.2	2.5	3.2	2.7	2.8	-	-	-	3.9	4.7	4.0	3.1	3.4	-	-	-	-	-
Rolandic operculum	-	3.8	3.3	-	-	-	3.4	2.8	-	-	2.6	5.2	5.3	-	-	-	-	-	-	-
Postcentral gyrus	-	3.2	2.4	-	-	-	4.0	-	-	-	-	5.3	3.2	2.4	-	-	-	-	-	-
Superior parietal gyrus	-	3.3	3.1	-	-	4.2	2.6	-	-	-	3.1	4.4	4.2	-	-	-	-	-	-	-
Inferior parietal, but supramarginal and angular gyri	-	4.1	3.7	2.8	-	-	3.1	-	-	-	2.4	5.4	4.9	2.9	-	-	-	-	-	-
Supramarginal gyrus	-	3.3	-	-	-	-	2.6	3.7	-	3.2	-	3.8	3.3	2.9	3.8	-	-	-	-	-
Angular gyrus	-	3.4	2.6	-	2.5	-	-	-	-	-	2.6	4.8	4.1	-	3.6	-	-	-	-	-
Precuneus	2.6	2.8	3.2	-	3.0	-	-	-	2.9	-	3.0	2.9	4.0	2.8	3.5	-	-	-	-	-
Superior occipital gyrus	-	3.6	2.8	2.7	4.2	2.5	2.7	4.3	-	-	-	5.1	5.2	2.8	2.7	-	-	-	-	4.0
Middle occipital gyrus	-	4.1	3.1	-	2.5	-	2.7	3.1	-	-	2.6	4.7	4.4	-	-	-	2.4	-	-	-
Inferior occipital gyrus	-	-	2.8	-	-	2.5	4.6	-	-	-	3.0	2.8	3.9	2.7	2.5	-	-	-	-	-
Calcarine fissure and surrounding cortex	-	3.3	3.3	-	-	-	-	3.8	-	-	-	2.9	5.3	-	-	-	2.6	-	-	-
Cuneus	-	2.8	3.4	2.7	4.5	2.7	-	-	-	-	-	4.1	3.9	-	3.6	-	-	-	-	3.4
Lingual gyrus	-	-	3.7	-	-	-	3.2	3.3	-	-	-	3.8	5.0	-	-	-	-	-	-	-
Fusiform gyrus	2.8	4.4	4.0	-	-	-	2.6	-	2.8	-	3.1	5.3	3.7	3.2	-	-	2.6	2.8	-	-
Heschl gyrus	-	3.5	3.2	-	-	2.8	3.0	-	-	-	3.3	5.3	3.6	-	2.5	-	-	-	-	-
Superior temporal gyrus	-	3.6	2.6	-	2.9	-	-	-	-	3.2	-	4.5	3.3	-	4.0	-	-	-	-	-
Middle temporal gyrus	-	4.1	3.1	3.0	-	-	-	2.7	-	-	-	4.4	4.5	2.7	-	-	2.7	-	-	-
Inferior temporal gyrus	-	3.1	5.0	3.3	-	-	-	-	-	-	-	3.3	4.9	3.4	-	-	-	3.5	-	-
Temporal pole: superior temporal gyrus	-	3.5	2.7	4.2	2.5	-	3.9	2.5	-	-	3.7	5.7	3.7	4.3	2.8	-	-	-	3.1	-
Temporal pole: middle temporal gyrus	2.8	-	3.0	4.3	-	2.5	3.4	-	-	-	4.4	3.9	4.3	4.1	-	-	-	-	3.2	-
Parahippocampal gyrus	3.0	3.3	3.0	3.4	-	2.6	3.8	-	3.6	-	4.6	5.4	3.4	5.1	-	-	-	-	-	-
Anterior cingulate and paracingulate gyri	-	2.4	-	3.2	-	-	3.0	-	-	-	-	3.4	2.5	4.1	-	-	-	-	-	-
Median cingulate and paracingulate gyri	-	-	3.7	-	2.8	3.2	-	-	-	-	3.6	3.8	3.4	-	3.1	-	-	2.7	-	-
Posterior cingulate gyrus	3.2	4.5	4.6	2.4	3.5	-	-	-	2.5	-	3.6	4.7	4.8	3.5	3.7	-	2.9	3.2	-	-
Insula	-	-	3.2	-	2.6	-	4.2	-	-	-	2.9	3.2	3.3	2.4	-	-	-	-	-	-
Hippocampus	-	-	2.6	2.5	-	3.7	4.9	-	2.6	3.4	3.2	3.7	3.6	2.9	3.5	-	-	-	-	-
Right Hemisphere																				
Gryus Rectus	-	-	2.7	-	-	3.8	3.7	-	-	-	2.9	4.0	4.1	-	-	-	-	-	-	-
Olfactory Cortex	-	3.2	3.4	3.6	-	-	2.7	3.0	-	-	-	4.9	4.9	3.2	2.4	-	-	-	-	-
Superior frontal gyrus, orbital part	-	3.0	-	3.5	2.4	-	-	-	-	-	3.0	3.7	3.1	3.5	3.2	-	-	-	-	-
Frontal gyrus, medial orbital part	-	3.4	-	4.2	2.5	-	4.1	3.1	2.6	4.1	2.8	5.0	3.5	5.1	3.5	-	-	-	2.5	-
Middle frontal gyrus, orbital part	-	3.0	-	2.7	2.6	2.8	5.1	2.9	-	-	2.6	4.5	4.5	3.3	2.8	-	-	-	-	-

(*continued on next page*)

Table 1 (*continued*)

ROIs	Pairwise Permutation Comparisons (FDR-corrected)																			
	Adults vs. Children					School vs. Preschool					Adults vs. Preschool					Adults vs. School				
Frequency Bands	δ	θ	α	β	γ	δ	θ	α	β	γ	δ	θ	α	β	γ	δ	θ	α	β	γ
Inferior frontal gyrus, orbital part	3.1	-	2.5	-	-	-	-	-	-	-	3.4	3.3	2.9	-	-	-	-	-	-	-
Superior frontal gyrus	3.0	2.9	3.7	3.0	-	2.6	-	2.8	-	-	4.3	3.8	5.0	3.1	-	-	-	-	-	-
Middle frontal gyrus	-	2.8	2.6	2.8	-	-	3.6	-	-	-	-	4.0	3.3	2.9	-	-	-	-	-	-
Inferior frontal gyrus, opercular part	-	2.8	2.9	3.3	-	-	3.3	2.6	-	-	2.6	4.4	3.6	3.7	-	-	-	-	-	-
Inferior frontal gyrus, triangular part	-	4.3	3.0	2.9	3.1	-	3.3	2.7	4.0	2.9	3.2	5.3	5.1	4.3	4.0	-	2.5	-	-	-
Superior frontal gyrus, medial	2.5	4.6	3.9	2.8	-	-	2.9	-	-	-	2.8	5.7	4.3	-	-	-	2.7	2.6	-	-
Supplementary motor area	-	4.9	3.7	-	2.8	-	3.0	-	-	-	-	6.1	3.1	-	2.6	-	3.1	2.9	-	-
Paracentral lobule	-	4.2	3.5	-	2.7	-	3.2	-	2.7	-	2.9	4.7	3.6	2.7	2.5	-	-	-	-	-
Precentral gyrus	-	3.0	-	3.9	-	-	-	-	-	-	2.4	3.5	-	3.8	2.7	-	-	-	2.6	-
Rolandic operculum	-	4.1	2.7	-	-	-	3.6	-	2.6	-	-	4.8	3.2	2.5	-	-	-	-	-	-
Postcentral gyrus	2.8	2.8	3.7	-	-	-	-	2.6	-	-	3.4	3.7	4.9	-	-	-	-	-	-	-
Superior parietal gyrus	-	2.6	2.5	-	-	-	3.5	-	-	-	2.4	3.6	3.1	-	-	-	-	-	-	-
Inferior parietal, but supramarginal and angular gyri	-	3.4	-	-	3.6	-	3.0	-	-	-	-	4.1	-	2.7	3.7	-	-	-	-	-
Supramarginal gyrus	-	3.7	-	2.6	-	2.5	3.0	-	-	-	-	4.7	2.9	2.6	2.9	-	-	-	-	-
Angular gyrus	-	3.6	3.8	2.9	-	3.5	-	-	-	-	2.9	4.0	3.4	2.9	-	-	-	2.8	-	-
Precuneus	-	3.5	-	-	-	2.8	-	-	-	-	3.1	3.4	3.1	-	-	-	-	-	-	-
Superior occipital gyrus	-	3.0	-	2.6	3.1	-	-	-	-	-	-	3.6	3.2	2.8	4.0	-	-	-	-	-
Middle occipital gyrus	-	3.8	2.6	-	-	2.5	-	-	-	-	2.9	3.7	3.2	-	-	-	2.7	-	-	-
Inferior occipital gyrus	-	2.8	3.0	2.7	3.0	-	-	-	-	-	3.5	3.5	3.4	-	3.0	-	-	-	-	-
Calcarine fissure and surrounding cortex	-	2.5	2.9	-	2.9	-	-	-	-	-	-	3.2	3.2	-	2.8	-	-	-	-	-
Cuneus	-	3.9	-	-	-	-	2.9	2.9	-	-	2.9	4.8	4.0	-	-	-	-	-	-	-
Lingual gyrus	-	2.7	-	3.2	-	-	-	-	-	-	3.0	3.1	3.5	3.4	2.8	-	-	-	-	-
Fusiform gyrus	-	3.0	2.5	4.6	-	2.6	3.5	-	-	-	2.4	4.5	2.9	4.3	-	-	-	-	3.2	-
Heschl gyrus	-	-	-	-	-	-	2.6	-	-	-	-	3.1	-	2.7	-	-	-	-	-	-
Superior temporal gyrus	-	3.2	-	-	-	-	-	-	3.4	-	-	3.6	-	3.2	2.7	-	-	-	-	-
Middle temporal gyrus	-	4.0	-	-	-	2.5	3.2	-	-	-	2.4	5.5	2.5	2.6	2.4	-	-	-	-	-
Inferior temporal gyrus	-	2.7	-	3.3	-	-	3.3	2.6	-	-	2.8	4.1	3.1	3.6	2.7	-	-	-	-	-
Temporal pole: superior temporal gyrus	-	2.9	2.5	2.6	3.4	-	2.9	4.0	-	3.3	-	4.8	4.1	2.9	4.7	-	-	-	-	-
Temporal pole: middle temporal gyrus	-	2.8	4.0	2.9	-	2.6	-	2.6	-	-	3.1	3.4	4.9	3.4	-	-	-	-	-	-
Parahippocampal gyrus	-	4.0	-	3.0	-	2.9	4.1	2.7	-	-	-	6.4	3.7	3.5	2.7	-	-	-	-	-
Anterior cingulate and paracingulate gyri	-	3.2	4.3	-	-	2.9	3.1	-	-	-	3.4	4.6	4.0	-	-	-	-	3.4	-	-
Median cingulate and paracingulate gyri	-	2.9	3.9	2.8	4.0	2.7	3.2	-	-	-	3.7	4.7	3.6	3.1	3.2	-	-	3.0	-	3.0
Posterior cingulate gyrus	-	4.0	2.6	3.3	-	2.6	-	-	2.5	-	-	3.7	2.9	4.7	-	-	2.8	-	-	-
Insula	-	2.7	-	-	-	-	2.5	-	-	-	2.5	4.3	-	2.4	-	-	-	-	-	-
Hippocampus	-	–3.8	–3.2	–3.5	–2.8	-	–2.6	-	-	-	-	–4.4	–3.1	–3.8	–2.6	-	-	-	-	-

2012). Thus, the adult brain may still be scale-free, although less so than that in children. During development, the hub regions might become less central, possibly as a protective mechanism, since disturbances and insults to the hub regions can produce lifelong changes in neurological and cognitive functioning. For instance, hub regions such as posterior and anterior cingulate, medial frontal and medial parietal areas are prone to damage in a wide variety of neurological diseases (Crossley et al., 2014; DeSalvo et al., 2014; Stam et al., 2009; Tewarie et al., 2014; Yu et al., 2017). The observed increase in Degree Correlation is suggestive of a developmental trend for hub regions to connect preferentially with each other (so-called "assortativeness"; Newman, 2003). The densely interconnected hub regions form a "rich-club" (van den Heuvel and Sporns, 2011), which has been shown to exist in the newborn human brain (Ball et al., 2014) and to further develop throughout adolescence (Dennis et al., 2013) conferring significant functional benefits upon the adult brain networks (Collin et al., 2014). Finally, our finding of increased Degree Correlation with age agrees with the widely accepted concept that, at the macroscopic level, the mature human brain is organised as an assortative network (Bettencourt et al., 2007; Stam and van Straaten, 2012). It is also in line with an EEG study reporting that functional brain networks are assortative (de Haan et al., 2009).

Our second aim was to explore whether the nodal centrality increases in hub regions and decreases in non-hub regions from childhood to adulthood. We found that Degree and Betweenness Centrality did not change, but Eccentricity increased significantly from children to adults. The overall increase in Eccentricity manifests in a distributed set of brain regions in all frequency bands. In theta mediated MSTs, all regions showed smaller Eccentricity in young children compared to adults. Specifically, we found regions in the fronto-parietal and default mode areas displayed the largest changes in Eccentricity across the five frequency bands. This is consistent with previous MST studies using scalp EEG, which reported age related decreases in nodal centrality (i.e., increase in Eccentricity and decrease in Degree and BC) in frontal-parietal electrodes from delta to alpha bands (Boersma et al., 2013; Toth et al., 2017). Our results suggest that these distributed regions become less central in the network, which also accords with the decreased scale-freeness of adults' networks as indicated by a smaller Kappa. We speculate that the decrease in nodal centrality may also reflect, to some extent, that during childhood brain regions become more inclined to connect with functionally related neighbours, rather than with distant regions. The decrease in Tree Hierarchy is harder to understand here, as a decrease is often observed in clinical groups (but see Janssen et al., 2017). Tree Hierarchy is a composite MST measure, and is correlated with changes in one or more MST measures (Stam et al., 2014). Given that Betweenness Centrality and Degree did not differ between children and adults, the observed decrease in Tree Hierarchy is likely to be driven by a decrease in Leaf Fraction. This finding also calls for a more straightforward quantification of network hierarchy in the field (see also limitations). Nevertheless, an increase in nodal Eccentricity and a decrease in Tree Hierarchy point to an increasingly segregated network with regional specialisation.

Consistent with our third hypothesis that network measures would be the most different in preschool years, all of our findings were significant when comparing the preschool children and older age groups (i.e., school children and adults), suggesting that the preschool years represents a unique and important period for network maturation. While young children have been largely under-represented in previous studies due to practical constraints, preschool years appear to represent a period of great cognitive and behavioural growth (Brown and Jernigan, 2012). It is therefore likely to constitute a sensitive period of brain development during which neuronal oscillations, inter-regional coupling, and network topology undergo significant changes.

Our fourth hypothesis predicted that network differences would share the same profile across five frequency bands between age groups. All global MST changes in our study were frequency-independent. Although the specific distributed regions that showed Eccentricity differences differed across frequency bands, there were also some frequency invariant differences: the largest number of regions that exhibited between group differences was found in theta and alpha mediated MSTs; regions in the fronto-parietal and default mode areas displayed the largest differences across all frequency bands and all pairwise age group comparisons. This seems to contradict some frequency-specific MST findings reported in lower frequency bands in previous developmental EEG studies. Possible reasons for these differences might be due to different imaging modalities (EEG versus MEG), eyes-open compared to eyes-closed resting-state status, sensor-space as opposed to source-space network analyses, and different functional connectivity metrics used (leakage-sensitive metrics such as synchronised likelihood versus leakage-invariant metrics such as PLI). Nevertheless, our results concur with other studies where the age-related differences on connectivity pattern and network configuration were found to be consistent across frequency bands (Barry et al., 2004; Bathelt et al., 2013; Murias et al., 2007), suggesting that similar network constraints manifest themselves across different physiological architectures.

Our results can be interpreted in a heuristic model of complex brain networks proposed by Stam and van Straaten (2012), which unifies the four powerful network models (i.e., regular, random, scale-free, and hierarchical modular models) into an abstract "network space" by representing a unique network property on each of the three axes: (1) Order – the horizontal axis that connects regular (high in order) and random networks (low in order) with the small-world network as the intermediate optimal model, indicating the balance between order and randomness; (2) Diversity – the vertical axis that connects scale-free (high in degree diversity) and random (low in degree diversity) networks, suggesting the presence of highly connected hubs; (3) Hierarchy – the diagonal axis that connects scale-free (high in hierarchy) and regular (low in hierarchy) networks, indicating the prevalence of modules clustered at different levels. Within this heuristic model of network space: (1) the smaller Diameter and larger Leaf Fraction in children compared to adults suggest that the functional brain networks become more segregated, shifting from a star-like towards a line-like configuration along the horizontal axis; (2) the larger Kappa and smaller Degree Correlation in children suggest that the networks move away from being scale-free along the vertical axis, in order to prevent the system from overloading hubs as well as to reduce vulnerability to random and targeted attacks (Stam et al., 2009); (3) the larger Tree Hierarchy and smaller Eccentricity of brain regions in children suggest a transition of functional brain networks along the diagonal axis towards the mature brain state which exhibits an optimal balance between functional integration and segregation.

There is a strong consensus that conventional graph theoretical metrics (such as the clustering coefficient and shortest path length) do not fully account for fundamental properties of brain networks, and the small-world model is often used inappropriately in the field of neuroscience (Papo et al., 2016). MST analysis, however, addresses methodological limitations such as biased estimates of network topology and biased network comparisons (Tewarie et al., 2015; van Wijk et al., 2010). We therefore propose a heuristic MST model space that characterises network topological change underlying typical brain development (Fig. 5). Within this MST model space, current findings suggest a clear developmental trajectory of brain networks along the right-vertical axis, suggesting a balance between integration and segregation in topology. A general framework for network development is provided by this network space, in which previous MST studies in developing populations can be interpreted. For instance, MST networks were found to be more star-like in ADHD children compared to age-matched typical children (Janssen et al., 2017), a pattern that could be characterised by a shift towards the lower-right corner of the network space. Such a trend indicates a delay in brain maturation for ADHD children. In contrast, MST networks become more line-like in children with dyslexia compared to typically developing children (Fraga Gonzalez et al., 2016), a transition to the lower-left corner of the network space. This pattern indicates an alternative

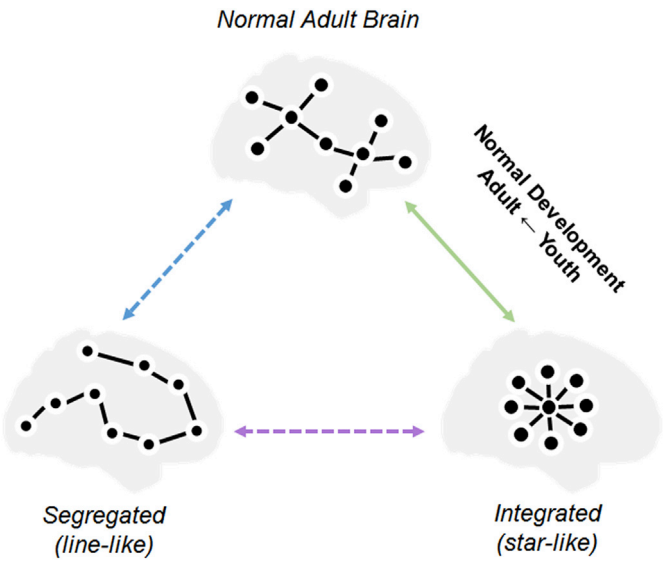

Fig. 5. A heuristic minimum spanning tree (MST) model for the emergence of complex brain networks. This MST model space is based on the heuristic model of complex brain networks proposed by Stam and van Straaten (2012). The model space consists of two extreme MSTs (representing network integration/segregation), an optimal MST for the normal adult brain, and three inter-connecting axes. Functional brain networks are proposed to develop from a star-like MST toward the optimal MST along the right-vertical axis (i.e., a balance between network integration and segregation). The solid line represents a developmental trajectory supported by this study; dashed lines represent trajectories that require future rigorous empirical support.

developmental trajectory along the horizontal axis for brain networks in dyslexia, veering off from the typical developmental trajectory which proceeds along the right-vertical axis. Our model space suggests that the normal adult brain that emerges during development is a special composite that combines optimal network integration and segregation, degree diversity, and hierarchy. Moreover, distinct pathological trajectories in adults, if projecting the normal adult brain onto the horizontal axis, could also be represented in this model space: a more line-like (de-centralised) MST was found in early relapsing remitting multiple sclerosis (Tewarie et al., 2014) and Alzheimer's disease patients (Yu et al., 2016), suggesting the networks move towards the lower-left corner (more segregated); and a more star-like (centralised) MST was observed in fronto-temporal dementia patients (Yu et al., 2016), indicating an opposite trend to the lower-right corner (more integrated).

In the present study, in order to overcome some of the limitations of earlier developmental studies on the network topology of young brains (Boersma et al., 2011; Boersma et al., 2013; Miskovic et al., 2015; Toth et al., 2017), and to provide a direct and unbiased measure of functional connectivity between brain sources across the whole brain, especially in preschool children, we have implemented several technical and methodological advances. First of all, we used age-appropriate MEG systems (i.e., a paediatric MEG for children under 6 years and a conventional MEG for school children and adults) to measure reference-free magnetic fields over the whole head, while subjects were situated in a quiet environment. Aside from being child-friendly due to its ease of participant preparation, MEG is particularly well suited to developmental studies since it is insensitive to age-related physiological and anatomical changes in biological tissues (e.g., bone thickness and density of the skull; Smith et al., 2012), which are interposed between the electrical sources and the MEG sensors. Secondly, it has been shown that sensor-level analysis can lead to spurious network results (Antiqueira et al., 2010; Lai et al., 2017). Therefore, we estimated MEG network organisation at the source level, using an advanced atlas-based MEG beamforming analysis pipeline (Hillebrand et al., 2012; Hillebrand et al., 2016). This also facilitates interpretation of our results in an anatomical context, and bridges between electrophysiological work and other neuroimaging methods such as those based on blood flow and oxygen metabolism (e.g. functional MRI). Thirdly, we utilised PLI to construct source level connectivity metrics for MST analysis. PLI only uses non-zero phase lags (see Methods for details) and therefore effectively ignores spurious connectivity due to field spread (Dominguez et al., 2007) and volume conduction/signal leakage (Lai et al., 2017; Schoffelen and Gross, 2009; Stam et al., 2007). Lastly, we used MST to perform unbiased network comparisons between different age groups (Tewarie et al., 2015; van Wijk et al., 2010). Moreover, we expect the effects of secondary leakage (Palva and Palva, 2012; Wang et al., 2018) on the estimated network metrics to be small due to the use of the PLI-based MST.

Nevertheless, there are few caveats worth mentioning in relation to the future application of this work. First of all, we defined our two child subgroups (preschool age: 4–6 years; and school age: 7–12 years) in the context of the child customised MEG, which is designed to fit approximately 90% of heads of 5-year old children (Johnson et al., 2010). This definition is also based on the culture specific schooling system; for example, in Australia, children must attend formal schooling when they turn 6 (or 6.5 for those whose birthdays are after 31 July), a year earlier than some European countries (Ailwood et al., 2016). With this potential difference in mind we subsequently analysed our data in child subgroups defined according to the "early childhood" definition of the United Nations Educational, Scientific and Cultural Organization, i.e., an "early childhood" (4–8 years) and a "late childhood" (9–12 years). Our supplementary analyses found the differences on the PLI and MST measures remained largely the same, suggesting the age differences reported in this paper were not driven by the grouping method we have used for our children sample (see Tables S1–3 in the Supplementary Materials). It is also conceivable that the significant differences we found between adults and children might have been caused by the large age range in our adult sample. In order to rule out this possibility, we conducted a separate re-analysis, where only adults aged below 35 years were included and compared with the preschool and school child subgroups. Again, the effects between adults and the preschool children remained unchanged in this re-analysis (see Tables S4–6 in the Supplementary Materials).

While our current cross-sectional data may provide valuable insights into average group changes with age, results reported here should be replicated in a large longitudinal sample with balanced gender members so that age-specific changes can be studied at an individual level for representative developmental trajectories for both males and females (given observed gender differences exists in brain development, e.g., Boersma et al., 2013).

To address technical concerns regarding the use of different MEG systems in a single study, we performed an additional analysis, where we reconstructed the adult gradiometer array to match the child gradiometer array. This analysis served to demonstrate that differences in sensor numbers across the two different MEG systems did not drive differences in the connectivity and network estimates of the brain activity that they recorded (see Tables S7 & 8 in the Supplementary Materials). Future neurodevelopmental MEG studies are likely to benefit from exciting breakthroughs in next-generation MEG systems, such as optically pumped magnetometers (OPMs; Boto et al., 2018). These might be used in flexible array configurations that allow for the use of single MEG systems across multiple age-groups, thereby avoiding potential confounds of age-related differences arising from system-specific requirements. In addition, while it would have been preferable to have a comparable amount of data in both adults and children, previously reported simulations demonstrate that beamformer performance (used in this analysis) plateaus before our lower data limit of ~96 s (24 epochs * 4.096s, Brookes et al., 2008) – this mitigates the concern that different amounts of data across groups could be a problem herein.

From a theoretical point of view, it is conceded that there are currently no simple mathematical models that optimally characterise properties of normal brain networks, such as hierarchical modularity, in order to fill the gap between the existing small-world and scale-free

network models. Tree Hierarchy is a composite measure on network hierarchy, and thus is inherently correlated with other measures such as leaf number and maximal betweenness centrality (see methods for details). Therefore, discovery and/or development of new mathematical models are likely to offer substantial support for the acquisition of a deeper understanding of various network constraints to the developing brain (Stam and van Straaten, 2012).

From a methodological point of view, although in the present study we carefully accounted for the signal leakage in source space using the leakage-invariant PLI metric, and loops were discarded in the MST construction, the data may still suffer to some extent from so-called secondary leakage (Palva and Palva, 2012; Wang et al., 2018). Therefore, future studies would also benefit from advanced methods such as Löwdin Orthogonalisation (Lowdin, 1950) to reduce those "ghost" connections (Colclough et al., 2015).

In regard to the MRI warping procedure used for anatomical co-registration in children, we initially tested with age-specific paediatric templates as it was suspected that in comparison to the adult template, paediatric templates would produce a better approximation to the child's brain anatomy due to better alignment in terms of skull thickness and brain morphology. However, adult and child templates produced very similar results in a previous study (Cheyne et al., 2014). Moreover, a recent MEG study showed that there is largely consistent relative power, connectivity, and network estimations between using surrogate template and native MRI co-registration of MEG (Douw et al., 2018). Additionally, AAL was not available for these paediatric templates, hence using the anatomical information from the AAL (adult) atlas (Tzourio-Mazoyer et al., 2002) with paediatric surrogate MRIs would still provide an approximate labelling that would be highly dependent on the quality of the digitised head surfaces. Therefore, the surrogate procedure (using the adult template), as well as the subsequent analyses, were kept the same for all participants. Nevertheless, the use of age-specific template brain images and atlases together with surface-based registration in further studies could help to minimise registration errors due to the heterogeneity of brain anatomy in young children (Fonov et al., 2011).

Lastly it is widely accepted that spontaneous neuronal oscillations change drastically with age, manifesting a decrease in the absolute spectral power, and an increase in the peak frequency of the dominant alpha band oscillation at rest (Gomez et al., 2017; Rodriguez-Martinez et al., 2017; Schafer et al., 2014). Thus, canonically-defined frequency bands may overlook some physiological mechanisms underlying the development of oscillatory neural networks. Estimating network properties from age-appropriate frequency bands is critical in future work (Boersma et al., 2013); for example, by parameterisation of neuronal power spectral densities on the basis of putative oscillatory components (Haller et al., 2018).

In conclusion, we demonstrated that functional brain networks become more segregated during childhood. Increases in MST Diameter and decreases in Leaf Fraction indicate that functional networks develop into a more line-like (de-centralised) topology; increases in Degree Centrality and Eccentricity suggest brain regions stay less central and become more locally specialised; decreases in Kappa and Tree Hierarchy emphasise that the network segregation during development balances the benefits of integration between distant brain regions against the risks of overload on central regions. Finally, these topological network changes are most evident in preschool years and exhibit the same pattern in the low-frequency delta through to the high frequency gamma bands.

Our data delineate a clear developmental trajectory of functional brain networks in typical children. If the current results can be replicated with a larger sample in a longitudinal design, such MST measures could be used as age-appropriate functional backbone references – "reference MSTs", against which patterns of brain networks in different age categories and in neurodevelopmental disorders could be systematically examined.

We propose a heuristic MST model for the emergence of complex brain networks, in which different patterns of network abnormality could be discerned depending upon their trajectories through this "network space". Therefore, our study represents the first attempt in providing a unifying network model for the development of functional brain networks in childhood. We anticipate new data from both normative and abnormal developmental studies to be incorporated into this network space to enable us not only to understand mechanism for early brain development, but most importantly to translate brain network studies into solutions for clinical diagnosis and treatment.

Author contributions

Wei He: conceptualisation, funding acquisition, data curation, formal analysis, validation, visualisation, methodology, writing (original draft, reviewing and editing); Paul F. Sowman: conceptualisation, funding acquisition, data collection, writing (reviewing and editing); Jon Brock: conceptualisation, funding acquisition, writing (reviewing and editing); Andrew C. Etchell: project management, data collection and curation; Cornelis J. Stam: conceptualisation, resources, methodology, writing (reviewing and editing); Arjan Hillebrand: conceptualisation, resources, formal analysis, validation, visualisation, methodology, supervision, writing (original draft, reviewing and editing).

Acknowledgements

We thank all participants for their participation. We also thank Douglas Cheyne and Cecilia Jobst for their assistance in the preliminary data analysis, and Craig Richardson for his technical support in establishing inter-institutional collaborative data analysis platform. Finally, we acknowledge the collaboration of Kanazawa Institute of Technology in establishing the KIT-Macquarie MEG laboratory. This work was supported by the Australian Research Council (ARC) Centre of Excellence in Cognition and its Disorders (grant number CE110001021, http://www.ccd.edu.au), and the ARC Discovery Project (DP170103148). Wei He was supported by the Macquarie University Research Fellowship (#9201501199). Paul F. Sowman was supported by the ARC Discovery Early Career Researcher Award (DE130100868) and the Australian National Health and Medical Research Council (#1003760).

Appendix A. Supplementary data

Supplementary data to this article can be found online at https://doi.org/10.1016/j.neuroimage.2019.06.055.

References

Ailwood, J., Boyd, W., Theobald, M., 2016. Understanding Early Childhood Education and Care in Australia: Practices and Perspectives. A & U Academic, Sydney, Australia.
Antiqueira, L., Rodrigues, F.A., van Wijk, B.C., Costa Lda, F., Daffertshofer, A., 2010. Estimating complex cortical networks via surface recordings - a critical note. Neuroimage 53 (2), 439–449.
Baillet, S., 2017. Magnetoencephalography for brain electrophysiology and imaging. Nat. Neurosci. 20 (3), 327–339.
Ball, G., Aljabar, P., Zebari, S., Tusor, N., Arichi, T., Merchant, N., et al., 2014. Rich-club organization of the newborn human brain. Proc. Natl. Acad. Sci. U. S. A. 111 (20), 7456–7461.
Barabasi, A.L., Albert, R., 1999. Emergence of scaling in random networks. Science 286 (5439), 509–512.
Barrat, A., Barthélemy, M., Vespignani, A., 2008. Dynamical Processes on Complex Networks. Cambridge University Press, Cambridge, UK.
Barry, R.J., Clarke, A.R., McCarthy, R., Selikowitz, M., Johnstone, S.J., Rushby, J.A., 2004. Age and gender effects in EEG coherence: I. Developmental trends in normal children. Clin. Neurophysiol. 115 (10), 2252–2258.
Bathelt, J., O'Reilly, H., Clayden, J.D., Cross, J.H., de Haan, M., 2013. Functional brain network organisation of children between 2 and 5 years derived from reconstructed activity of cortical sources of high-density EEG recordings. Neuroimage 82, 595–604.
Baum, G.L., Ciric, R., Roalf, D.R., Betzel, R.F., Moore, T.M., Shinohara, R.T., et al., 2017. Modular segregation of structural brain networks supports the development of executive function in youth. Curr. Biol. 27 (11), 1561–1572 e1568.
Benjamini, Y., Hochberg, Y., 1995. Controlling the false discovery rate: a practical and powerful approach to multiple testing. J. R. Stat. Soc. Ser. B (Methodol.) 289–300.
Bettencourt, L.M., Stephens, G.J., Ham, M.I., Gross, G.W., 2007. Functional structure of cortical neuronal networks grown in vitro. Phys. Rev.: Stat. Nonlinear Soft Matter Phys. 75 (2 Pt 1), 021915.

Boersma, M., Smit, D.J., Boomsma, D.I., De Geus, E.J., Delemarre-van de Waal, H.A., Stam, C.J., 2013. Growing trees in child brains: graph theoretical analysis of electroencephalography-derived minimum spanning tree in 5- and 7-year-old children reflects brain maturation. Brain Connect. 3 (1), 50–60.
Boersma, M., Smit, D.J., de Bie, H.M., Van Baal, G.C., Boomsma, D.I., de Geus, E.J., et al., 2011. Network analysis of resting state EEG in the developing young brain: structure comes with maturation. Hum. Brain Mapp. 32 (3), 413–425.
Boto, E., Holmes, N., Leggett, J., Roberts, G., Shah, V., Meyer, S.S., Brookes, M.J., 2018. Moving magnetoencephalography towards real-world applications with a wearable system. Nature 555 (7698), 657–661.
Brookes, M.J., Vrba, J., Robinson, S.E., Stevenson, C.M., Peters, A.M., Barnes, G.R., et al., 2008. Optimising experimental design for MEG beamformer imaging. Neuroimage 39 (4), 1788–1802.
Brown, T.T., Jernigan, T.L., 2012. Brain development during the preschool years. Neuropsychol. Rev. 22 (4), 313–333.
Bullmore, E., Barnes, A., Bassett, D.S., Fornito, A., Kitzbichler, M., Meunier, D., Suckling, J., 2009. Generic aspects of complexity in brain imaging data and other biological systems. Neuroimage 47 (3), 1125–1134.
Bullmore, E., Sporns, O., 2012. The economy of brain network organization. Nat. Rev. Neurosci. 13 (5), 336–349.
Buzsaki, G., 2006. Rhythms of the Brain. Oxford University Press, Oxford, UK.
Buzsaki, G., Draguhn, A., 2004. Neuronal oscillations in cortical networks. Science 304 (5679), 1926–1929.
Cao, M., He, Y., Dai, Z., Liao, X., Jeon, T., Ouyang, M., et al., 2017. Early development of functional network segregation revealed by connectomic analysis of the preterm human brain. Cerebr. Cortex 27 (3), 1949–1963.
Cheyne, D., Bostan, A.C., Gaetz, W., Pang, E.W., 2007. Event-related beamforming: a robust method for presurgical functional mapping using MEG. Clin. Neurophysiol. 118 (8), 1691–1704.
Cheyne, D., Jobst, C., Tesan, G., Crain, S., Johnson, B., 2014. Movement-related neuromagnetic fields in preschool age children. Hum. Brain Mapp. 35 (9), 4858–4875.
Cole, M.W., Yarkoni, T., Repovš, G., Anticevic, A., Braver, T.S., 2012. Global connectivity of prefrontal cortex predicts cognitive control and intelligence. J. Neurosci. 32 (26), 8988–8999.
Colclough, G.L., Brookes, M.J., Smith, S.M., Woolrich, M.W., 2015. A symmetric multivariate leakage correction for MEG connectomes. Neuroimage 117, 439–448.
Collin, G., Sporns, O., Mandl, R.C., van den Heuvel, M.P., 2014. Structural and functional aspects relating to cost and benefit of rich club organization in the human cerebral cortex. Cerebr. Cortex 24 (9), 2258–2267.
Crossley, N.A., Mechelli, A., Scott, J., Carletti, F., Fox, P.T., McGuire, P., Bullmore, E.T., 2014. The hubs of the human connectome are generally implicated in the anatomy of brain disorders. Brain 137 (Pt 8), 2382–2395.
de Haan, W., Pijnenburg, Y.A., Strijers, R.L., van der Made, Y., van der Flier, W.M., Scheltens, P., Stam, C.J., 2009. Functional neural network analysis in frontotemporal dementia and Alzheimer's disease using EEG and graph theory. BMC Neurosci. 10 (101).
Dennis, E.L., Jahanshad, N., Toga, A.W., McMahon, K.L., de Zubicaray, G.I., Hickie, I., et al., 2013. Development of the "rich club" in brain connectivity networks from 438 adolescents and adults aged 12 to 30. Proc. IEEE Int. Symp. Biomed. Imaging 624–627.
DeSalvo, M.N., Douw, L., Tanaka, N., Reinsberger, C., Stufflebeam, S.M., 2014. Altered structural connectome in temporal lobe epilepsy. Radiology 270 (3), 842–848.
Dominguez, L.G., Wennberg, R., Velazquez, J.L.P., Erra, R.G., 2007. Enhanced measured synchronization of unsynchronized sources: inspecting the physiological significance of synchronization analysis of whole brain electrophysiological recordings. Int. J. Phys. Sci. 2 (11), 305–317.
Douw, L., Nieboer, D., Stam, C.J., Tewarie, P., Hillebrand, A., 2018. Consistency of magnetoencephalographic functional connectivity and network reconstruction using a template versus native MRI for coregistration. Hum. Brain Mapp. 39 (1), 104–119.
Douw, L., Schoonheim, M.M., Landi, D., van der Meer, M.L., Geurts, J.J., Reijneveld, J.C., et al., 2011. Cognition is related to resting-state small-world network topology: an magnetoencephalographic study. Neuroscience 175, 169–177.
Erdös, P., Rényi, A., 1959. On random graphs. Publ. Math. 6, 290–297.
Fair, D.A., Cohen, A.L., Power, J.D., Dosenbach, N.U., Church, J.A., Miezin, F.M., et al., 2009. Functional brain networks develop from a "local to distributed" organization. PLoS Comput. Biol. 5 (5), e1000381.
Fair, D.A., Dosenbach, N.U., Church, J.A., Cohen, A.L., Brahmbhatt, S., Miezin, F.M., et al., 2007. Development of distinct control networks through segregation and integration. Proc. Natl. Acad. Sci. U. S. A. 104 (33), 13507–13512.
Fonov, V., Evans, A.C., Botteron, K., Almli, C.R., McKinstry, R.C., Collins, D.L., Brain Development Cooperative, G., 2011. Unbiased average age-appropriate atlases for pediatric studies. Neuroimage 54 (1), 313–327.
Fornito, A., Zalesky, A., Bassett, D.S., Meunier, D., Ellison-Wright, I., Yucel, M., et al., 2011. Genetic influences on cost-efficient organization of human cortical functional networks. J. Neurosci. 31 (9), 3261–3270.
Fraga Gonzalez, G., Van der Molen, M.J.W., Zaric, G., Bonte, M., Tijms, J., Blomert, L., et al., 2016. Graph analysis of EEG resting state functional networks in dyslexic readers. Clin. Neurophysiol. 127 (9), 3165–3175.
Friston, K.J., 1994. Functional and effective connectivity in neuroimaging: a synthesis. Hum. Brain Mapp. 2 (1–2), 56–78.
Gomez, C.M., Rodriguez-Martinez, E.I., Fernandez, A., Maestu, F., Poza, J., Gomez, C., 2017. Absolute power spectral density changes in the magnetoencephalographic activity during the transition from childhood to adulthood. Brain Topogr. 30 (1), 87–97.
Grayson, D.S., Fair, D.A., 2017. Development of large-scale functional networks from birth to adulthood: a guide to the neuroimaging literature. Neuroimage 160, 15–31.
Haller, M., Donoghue, T., Peterson, E., Varma, P., Sebastian, P., Gao, R., et al., 2018. Parameterizing Neural Power Spectra. bioRxiv, p. 299859.
He, W., Brock, J., Johnson, B.W., 2014. Face-sensitive brain responses measured from a four-year-old child with a custom-sized child MEG system. J. Neurosci. Methods 222, 213–217.
Hedges, L.V., 1981. Distribution theory for Glass's estimator of effect size and related estimators. J. Educ. Stat. 6 (2), 107–128.
Hillebrand, A., Barnes, G.R., 2005. Beamformer analysis of MEG data. Int. Rev. Neurobiol. 68, 149–171.
Hillebrand, A., Barnes, G.R., Bosboom, J.L., Berendse, H.W., Stam, C.J., 2012. Frequency-dependent functional connectivity within resting-state networks: an atlas-based MEG beamformer solution. Neuroimage 59 (4), 3909–3921.
Hillebrand, A., Tewarie, P., van Dellen, E., Yu, M., Carbo, E.W., Douw, L., et al., 2016. Direction of information flow in large-scale resting-state networks is frequency-dependent. Proc. Natl. Acad. Sci. Unit. States Am. 113 (14), 3867–3872.
Huang, M.X., Mosher, J.C., Leahy, R.M., 1999. A sensor-weighted overlapping-sphere head model and exhaustive head model comparison for MEG. Phys. Med. Biol. 44 (2), 423–440.
Janssen, T.W.P., Hillebrand, A., Gouw, A., Gelade, K., Van Mourik, R., Maras, A., Oosterlaan, J., 2017. Neural network topology in ADHD; evidence for maturational delay and default-mode network alterations. Clin. Neurophysiol. 128 (11), 2258–2267.
Johnson, B.W., Crain, S., Thornton, R., Tesan, G., Reid, M., 2010. Measurement of brain function in pre-school children using a custom sized whole-head MEG sensor array. Clin. Neurophysiol. 121 (3), 340–349.
Kado, H., Higuchi, M., Shimogawara, M., Haruta, Y., Adachi, Y., Kawai, J., et al., 1999. Magnetoencephalogram systems developed at KIT. IEEE Trans. Appl. Supercond. 9 (2), 4057–4062.
Kruskal, J., 1956. On the shortest spanning subtree of a graph and the traveling salesman problem. Proc. Am. Math. Soc. 7 (1), 48–50.
Lai, M., Demuru, M., Hillebrand, A., Fraschini, M., 2017. A Comparison between Scalp-And Source-Reconstructed EEG Networks. bioRxiv, p. 121764.
Lowdin, P.O., 1950. On the non-orthogonality problem connected with the use of atomic wave functions in the theory of molecules and crystals. J. Chem. Phys. 18, 365–375.
Marek, S., Hwang, K., Foran, W., Hallquist, M.N., Luna, B., 2015. The contribution of network organization and integration to the development of cognitive control. PLoS Biol. 13 (12), e1002328.
Marple, S.L., 1999. Computing the discrete-time "analytic" signal via FFT. IEEE Trans. Signal Process. 47 (9), 2600–2603.
Meunier, D., Lambiotte, R., Fornito, A., Ersche, K.D., Bullmore, E.T., 2009. Hierarchical modularity in human brain functional networks. Front. Neuroinf. 3, 37.
Miskovic, V., Ma, X., Chou, C.A., Fan, M., Owens, M., Sayama, H., Gibb, B.E., 2015. Developmental changes in spontaneous electrocortical activity and network organization from early to late childhood. Neuroimage 118, 237–247.
Mulder, H.M., 1992. Julius Petersen's theory of regular graphs. Discrete Math. 100 (1), 157–175.
Murias, M., Swanson, J.M., Srinivasan, R., 2007. Functional connectivity of frontal cortex in healthy and ADHD children reflected in EEG coherence. Cerebr. Cortex 17 (8), 1788–1799.
Newman, M.E.J., 2003. Mixing patterns in networks. Phys. Rev. 67 (2), 026126.
Newman, M.E.J., 2010. Networks: an Introduction. Oxford University Press, Oxford, UK.
Palva, S., Palva, J.M., 2012. Discovering oscillatory interaction networks with M/EEG: challenges and breakthroughs. Trends Cognit. Sci. 16 (4), 219–230.
Papo, D., Zanin, M., Martinez, J.H., Buldu, J.M., 2016. Beware of the small-world neuroscientist! Front. Hum. Neurosci. 10, 96.
Power, J.D., Cohen, A.L., Nelson, S.M., Wig, G.S., Barnes, K.A., Church, J.A., et al., 2011. Functional network organization of the human brain. Neuron 72 (4), 665–678.
Rapaport, H., Seymour A., R., Sowman F., P., Stylianou, E., Johnson W., B., Crain, S., He, W., 2019. Studying Brain Function in Children Using Magnetoencephalography. Journal of Visualised Experiments. https://doi.org/10.3791/58909.
Robinson, S.E., 1999. Functional neuroimaging by synthetic aperture magnetometry (SAM). Recent Adv. Biomagn. 302–305.
Rodriguez-Martinez, E.I., Ruiz-Martinez, F.J., Barriga Paulino, C.I., Gomez, C.M., 2017. Frequency shift in topography of spontaneous brain rhythms from childhood to adulthood. Cognit. Neurodynamics 11 (1), 23–33.
Schafer, C.B., Morgan, B.R., Ye, A.X., Taylor, M.J., Doesburg, S.M., 2014. Oscillations, networks, and their development: MEG connectivity changes with age. Hum. Brain Mapp. 35 (10), 5249–5261.
Schoffelen, J.M., Gross, J., 2009. Source connectivity analysis with MEG and EEG. Hum. Brain Mapp. 30 (6), 1857–1865.
Smith, K., Politte, D., Reiker, G., Nolan, T.S., Hildebolt, C., Mattson, C., et al., 2012. Automated measurement of pediatric cranial bone thickness and density from clinical computed tomography. Conf. Proc. IEEE Eng. Med. Biol. Soc. 2012, 4462–4465.
Sporns, O., 2011. Networks of the Brain. The MIT Press, Cambridge, Massachusetts, USA.
Sporns, O., 2013. Structure and function of complex brain networks. Dialogues Clin. Neurosci. 15 (3), 247–262.
Stam, C.J., 2014. Modern network science of neurological disorders. Nat. Rev. Neurosci. 15 (10), 683–695.
Stam, C.J., de Haan, W., Daffertshofer, A., Jones, B.F., Manshanden, I., van Cappellen van Walsum, A.M., et al., 2009. Graph theoretical analysis of magnetoencephalographic functional connectivity in Alzheimer's disease. Brain 132 (Pt 1), 213–224.
Stam, C.J., Nolte, G., Daffertshofer, A., 2007. Phase lag index: assessment of functional connectivity from multi channel EEG and MEG with diminished bias from common sources. Hum. Brain Mapp. 28 (11), 1178–1193.
Stam, C.J., Tewarie, P., Van Dellen, E., van Straaten, E.C., Hillebrand, A., Van Mieghem, P., 2014. The trees and the forest: characterization of complex brain networks with minimum spanning trees. Int. J. Psychophysiol. 92 (3), 129–138.

Stam, C.J., van Straaten, E.C.W., 2012. The organization of physiological brain networks. Clin. Neurophysiol. 123 (6), 1067–1087.
Tewarie, P., Hillebrand, A., Schoonheim, M.M., van Dijk, B.W., Geurts, J.J., Barkhof, F., et al., 2014. Functional brain network analysis using minimum spanning trees in Multiple Sclerosis: an MEG source-space study. Neuroimage 88, 308–318.
Tewarie, P., van Dellen, E., Hillebrand, A., Stam, C.J., 2015. The minimum spanning tree: an unbiased method for brain network analysis. Neuroimage 104, 177–188.
Toth, B., Urban, G., Haden, G.P., Mark, M., Torok, M., Stam, C.J., Winkler, I., 2017. Large-scale network organization of EEG functional connectivity in newborn infants. Hum. Brain Mapp. 38 (8), 4019–4033.
Troebinger, L., Lopez, J.D., Lutti, A., Bestmann, S., Barnes, G., 2014. Discrimination of cortical laminae using MEG. Neuroimage 102 (Pt 2), 885–893.
Tzourio-Mazoyer, N., Landeau, B., Papathanassiou, D., Crivello, F., Etard, O., Delcroix, N., et al., 2002. Automated anatomical labeling of activations in SPM using a macroscopic anatomical parcellation of the MNI MRI single-subject brain. Neuroimage 15 (1), 273–289.
Uhlhaas, P.J., Roux, F., Rodriguez, E., Rotarska-Jagiela, A., Singer, W., 2010. Neural synchrony and the development of cortical networks. Trends Cognit. Sci. 14 (2), 72–80.
van Dellen, E., Sommer, I.E., Bohlken, M.M., Tewarie, P., Draaisma, L., Zalesky, A., et al., 2018. Minimum spanning tree analysis of the human connectome. Hum. Brain Mapp. 39 (6), 2455–2471.
van den Heuvel, M.P., Kersbergen, K.J., de Reus, M.A., Keunen, K., Kahn, R.S., Groenendaal, F., et al., 2015. The neonatal connectome during preterm brain development. Cerebr. Cortex 25 (9), 3000–3013.
van den Heuvel, M.P., Sporns, O., 2011. Rich-club organization of the human connectome. J. Neurosci. 31 (44), 15775–15786.
van den Heuvel, M.P., Stam, C.J., Boersma, M., Hulshoff Pol, H.E., 2008. Small-world and scale-free organization of voxel-based resting-state functional connectivity in the human brain. Neuroimage 43 (3), 528–539.
Van Diessen, E., Numan, T., Van Dellen, E., Van Der Kooi, A.W., Boersma, M., Hofman, D.,, et al., 2015. Opportunities and methodological challenges in EEG and MEG resting state functional brain network research. Clin. Neurophysiol. 126 (8), 1468–1481.
Van Mieghem, P., Magdalena, S.M., 2005. Phase transition in the link weight structure of networks. Phys. Rev. 72 (5), 056138.
Van Mieghem, P., van Langen, S., 2005. Influence of the link weight structure on the shortest path. Phys. Rev. 71 (5), 056113.
Van Mieghem, P., Wang, H., Ge, X., Tang, S., Kuipers, F.A., 2010. Influence of assortativity and degree-preserving rewiring on the spectra of networks. Eur. Phys. J. B 76 (4), 643–652.
van Wijk, B.C., Stam, C.J., Daffertshofer, A., 2010. Comparing brain networks of different size and connectivity density using graph theory. PLoS One 5 (10), e13701.
Wang, H., Hernandez, J.M., Van Mieghem, P., 2008. Betweenness centrality in a weighted network. Phys. Rev. 77 (4), 046105.
Wang, J., Wang, L., Zang, Y., Yang, H., Tang, H., Gong, Q., et al., 2009. Parcellation-dependent small-world brain functional networks: a resting-state fMRI study. Hum. Brain Mapp. 30 (5), 1511–1523.
Wang, S.H., Lobier, M., Siebenhuhner, F., Puolivali, T., Palva, S., Palva, J.M., 2018. Hyperedge bundling: a practical solution to spurious interactions in MEG/EEG source connectivity analyses. Neuroimage 173, 610–622.
Watts, D.J., Strogatz, S.H., 1998. Collective dynamics of 'small-world' networks. Nature 393 (6684), 440–442.
Weiskopf, N., Lutti, A., Helms, G., Novak, M., Ashburner, J., Hutton, C., 2011. Unified segmentation based correction of R1 brain maps for RF transmit field inhomogeneities (UNICORT). Neuroimage 54 (3), 2116–2124.
Wig, G.S., 2017. Segregated systems of human brain networks. Trends Cognit. Sci. 21 (12), 981–996.
Yap, P.T., Fan, Y., Chen, Y., Gilmore, J.H., Lin, W., Shen, D., 2011. Development trends of white matter connectivity in the first years of life. PLoS One 6 (9), e24678.
Yu, M., Engels, M.M.A., Hillebrand, A., van Straaten, E.C.W., Gouw, A.A., Teunissen, C., et al., 2017. Selective impairment of hippocampus and posterior hub areas in Alzheimer's disease: an MEG-based multiplex network study. Brain 140 (5), 1466–1485.
Yu, M., Gouw, A.A., Hillebrand, A., Tijms, B.M., Stam, C.J., van Straaten, E.C., Pijnenburg, Y.A., 2016. Different functional connectivity and network topology in behavioral variant of frontotemporal dementia and Alzheimer's disease: an EEG study. Neurobiol. Aging 42, 150–162.